Energy & Environmental Science

ROYAL SOCIETY OF CHEMISTRY

PAPER

View Article Online
View Journal | View Issue



Cite this: *Energy Environ. Sci.*, 2024, **17**, 3136

# Reversible solid bromine complexation into $Ti_3C_2T_x$ MXene carriers: a highly active electrode for bromine-based flow batteries with ultralow self-discharge†

Luyin Tang,[ab] Tianyu Li,[a] Wenjing Lu*[a] and Xianfeng Li*[a]

Bromine-based flow batteries (Br-FBs) are appealing for stationary energy storage because of their high energy density and low cost. However, the wider application of Br-FBs is hindered by the sluggish reaction kinetics of the $Br_2/Br^-$ redox couple and serious bromine crossover. Adding bromine complexing agents (BCAs) into electrolytes can inhibit bromine crossover effectively, but it generally deteriorates the reaction kinetics. Here, we use hexadecyl trimethyl ammonium bromide (CTAB) to intercalate $Ti_3C_2T_x$ MXene as electrodes for Br-FBs. In this design, CTAB acts as the BCA to form robust solid bromine complexes, which are accompanied by highly active $Ti_3C_2T_x$ MXene carriers. Soluble bromine species diffusion is perfectly suppressed based on such a strong and reversible solid complexation effect, while the adverse effect of solid complexes on reaction kinetics is well overcome. Thus, the assembled zinc-bromine flow battery delivered a remarkable improvement in suppressing self-discharge, achieving an unprecedently high capacity retention rate of 82.93% after standing for 24 h at 80 mA $cm^{-2}$. At a high current density of 180 mA $cm^{-2}$, this battery exhibited the highest voltage efficiency of 66.76% and energy efficiency of 66.06% ever reported, and also showed an outstanding long-term durability for 580 cycles with a high coulombic efficiency of 99.30%. This work provides a new strategy for designing electrodes with ultralow self-discharge, high power density and long cycle life for Br-FBs.

Received 5th February 2024,
Accepted 28th March 2024

DOI: 10.1039/d4ee00580e

rsc.li/ees



## Broader context

Bromine-based flow batteries (Br-FBs) are gaining increasing attention due to their high energy density and cost effectiveness. Nevertheless, the sluggish reaction kinetics of the $Br_2/Br^-$ redox couple and the serious self-discharge caused by the diffusion/crossover of soluble bromine species lead to low power density and severe capacity fading, constraining the widespread application of Br-FBs. Consequently, the robust and reversible solid complexation effect of bromine complexing agents is incorporated into electrodes, endowing Br-FBs with ultralow self-discharge. We use hexadecyl trimethyl ammonium bromide to intercalate highly catalytic $Ti_3C_2T_x$ MXene carriers, which can form solid complexes with bromine species. Meanwhile, $Ti_3C_2T_x$ MXene carriers exhibit low adsorption energy to bromine, accelerating the kinetics of $Br_2/Br^-$ reactions. Remarkably, a record high capacity retention rate of 82.93% after standing for 24 h at 80 mA $cm^{-2}$ is achieved for a Br-FB. At a high current density of up to 180 mA $cm^{-2}$, this Br-FB achieves the highest voltage efficiency and energy efficiency ever reported. This unique design breaks the "trade-off" between high bromine retention capacity and fast reaction kinetics. As a result, this work provides valuable insights into the design of high-performance electrodes for Br-FBs with ultralow self-discharge and high power density.

## Introduction

The huge demand for wide application of renewable resources such as solar energy has promoted the rapid development of energy storage technologies, which can ensure a stable electricity output and improve the grid safety and reliability.[1–4] Among various energy storage systems, bromine-based flow batteries (Br-FBs) have emerged as compelling candidates for stationary energy storage because of their high energy density

[a] *Dalian Institute of Chemical Physics, Chinese Academy of Sciences, Zhongshan Road 457, Dalian 116023, P. R. China. E-mail: luwenjing@dicp.ac.cn, lixianfeng@dicp.ac.cn*

[b] *University of Chinese Academy of Sciences, Beijing 100049, P. R. China*

† Electronic supplementary information (ESI) available. See DOI: https://doi.org/10.1039/d4ee00580e

and low cost.[5–7] Nevertheless, the bromine diffusion/crossover issue leads to severe self-discharge, decreasing the efficiencies, capacity and cycle life of Br-FBs. Additionally, the sluggish reaction kinetics of the $Br_2/Br^-$ redox couple results in a low working current density and power density of batteries.[8–10] To address the bromine diffusion/crossover issue, the common strategy is to introduce bromine complexing agents (BCAs) into electrolytes, which generally contain quaternary ammonium bromide groups, such as *N*-methylethylpyrrolidinium bromide (MEPBr).[11–13] BCAs will complex with soluble bromine species to form an oily polybromide phase, decreasing the bromine concentration in the aqueous phase. Moreover, it is easier for the as-formed bromine complexes with larger sizes to be excluded through a frequently used size-sieving membrane, improving the coulombic efficiency (CE) and capacity retention rate of the battery.[14,15]

However, the formation of the oily polybromide phase lowers the electrolyte conductivity and uniformity, deteriorating the reaction kinetics of the $Br_2/Br^-$ redox couple.[15–17] To address such a "trade-off" between inhibiting bromine diffusion and boosting reaction kinetics, our group has devoted great efforts to constructing highly electrochemically active electrodes with high bromine entrapping/retention capacity.[8,18,19] In particular, such electrode materials can play the same roles as BCAs, helping in constructing BCA-free Br-FBs with low self-discharge, high power density and long lifespan. We have used the adsorption and spatial confinement effects of porous carbon nitride nanosheets or vertically aligned $MoS_2$ nanosheet arrays to successfully endow the electrodes with high catalytic activity and high bromine retention capacity at the same time.[18,19] Nonetheless, the adsorption effect is not robust enough to retain bromine more sufficiently, while the spatial confinement effect seriously depends on the precise size control.

Herein, we directly introduced BCAs into the electrode, which entrap/retain bromine species in the electrode based on the strong and reversible solid complexation effect (Scheme 1). In this design, $Ti_3C_2T_x$ MXene served as a carrier to combine hexadecyl trimethyl ammonium bromide (CTAB) with a non-polar carbon felt (PCF) substrate by intercalation (Scheme 1). CTAB could complex with bromine species to form stable solid complexes instead of conventional oily complexes (Fig. S1 and S2, ESI†).[13,20] The interlayer spacing of $Ti_3C_2T_x$ MXene carriers was enlarged by CTAB intercalation, allowing the free entrance of $Br^-$ ions into their interlayers during the charge process. The oxidized and soluble $Br_n^-$ sequentially complexed with $CTA^+$ to form solid $CTA^+$–$Br_n^-$ complexes, which were stored in the interlayers of $Ti_3C_2T_x$ MXenes (Scheme 1). The bromine crossover issue was thereby effectively suppressed. Additionally, the $Ti_3C_2T_x$ MXene exhibited a strong adsorption effect on bromine species, boosting the rate-determining step of $Br_2/Br^-$ reactions.[21] The "trade-off" between inhibiting bromine diffusion and boosting reaction kinetics was consequently well overcome. Using $Ti_3C_2T_x$-CTAB decorated PCF substrate as the cathode, the assembled zinc–bromine flow battery (ZBFB) exhibited an extremely high capacity retention rate of 82.93% after the 24-h standing test at 80 mA $cm^{-2}$, much higher than those based on the adsorption effect or the spatial confinement effect.[18,19] At 180 mA $cm^{-2}$, this ZBFB exhibited a high voltage efficiency (VE) of 66.76% and a high energy efficiency (EE) of 66.06%, which could also run stably for over 580 cycles. Notably, the VE and EE were the highest values ever reported for ZBFBs (Table S1, ESI†). As a result, the strategy of incorporating the robust solid bromine complexation effect into electrodes can open up a new avenue for the application of Br-FBs with ultralow self-discharge, high power density and long lifespan.

## Results and discussion

### Rational design of CTAB intercalation into $Ti_3C_2T_x$ MXene

The intercalation of CTAB into $Ti_3C_2T_x$ MXene carriers was realized using a one-step method, as shown in Fig. S3 and S4 (ESI†). X-ray diffraction (XRD) patterns revealed that after being intercalated by CTAB, the (002) peak of $Ti_3C_2T_x$ MXene shifted from 8.55° to 7.2°, indicating the extended interlayer spacing from 1.0 nm to 1.2 nm (Fig. 1a and Fig. S5, ESI†).[22,23] The scanning electron microscopy (SEM) images clearly suggested the successful fabrication of $Ti_3C_2T_x$ MXene nanosheets from $Ti_3AlC_2$ powders (Fig. 1b and c). After being intercalated by

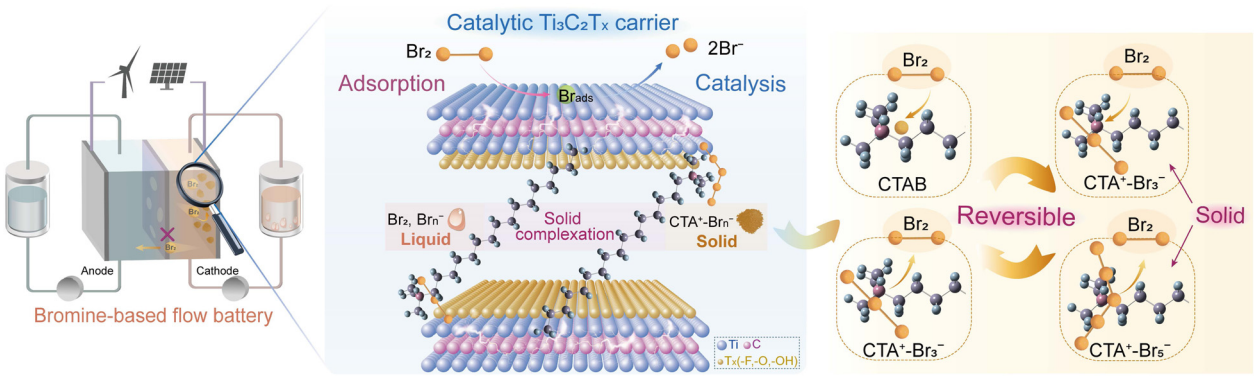


Scheme 1 Illustration of the $Ti_3C_2T_x$-CTAB decorated electrode with high catalytic activity and excellent bromine retention capacity for a Br-FB with ultralow self-discharge and a long lifespan.

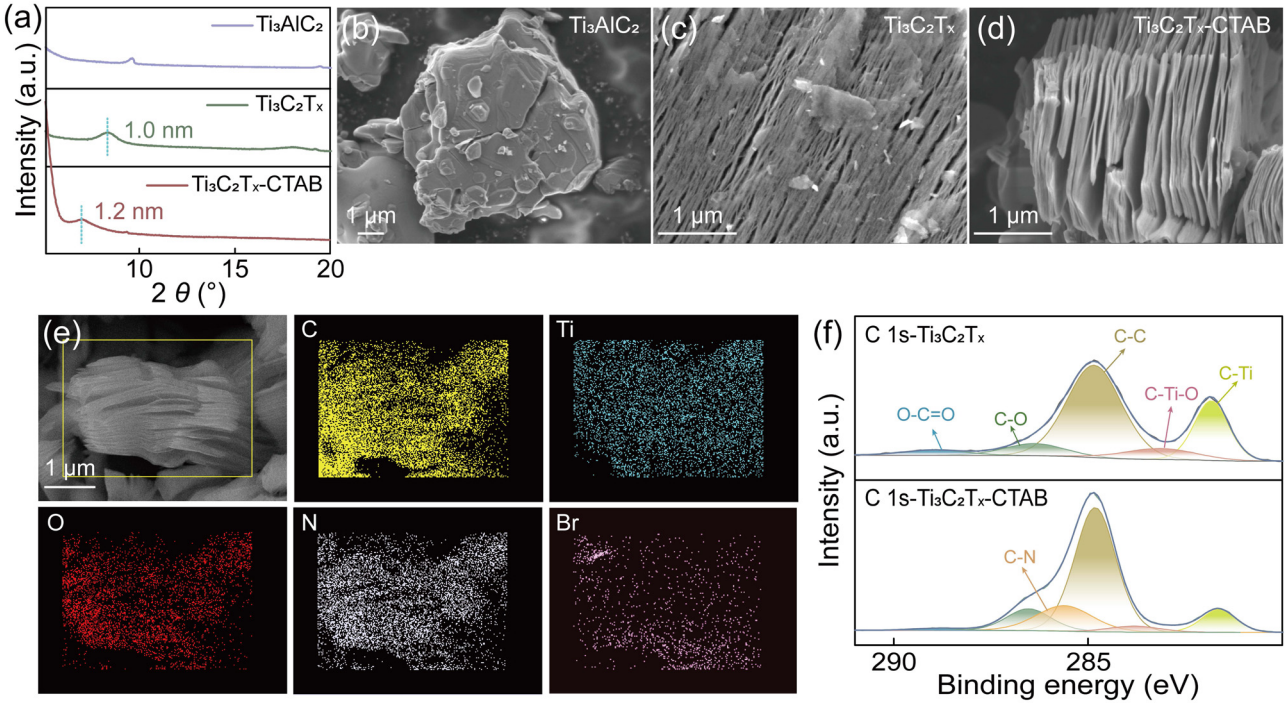


Fig. 1 Characterization of $Ti_3C_2T_x$-CTAB. (a) The XRD patterns of $Ti_3AlC_2$, $Ti_3C_2T_x$ and $Ti_3C_2T_x$-CTAB. (b)–(d) SEM images of $Ti_3AlC_2$, $Ti_3C_2T_x$ and $Ti_3C_2T_x$-CTAB. (e) EDS mappings of $Ti_3C_2T_x$-CTAB. (f) High-resolution C 1s XPS spectra of $Ti_3C_2T_x$ and $Ti_3C_2T_x$-CTAB.

CTAB, the laminated structure of $Ti_3C_2T_x$-CTAB was more obvious with a larger interlayer spacing, supporting XRD analysis (Fig. 1d). Moreover, compared with $Ti_3C_2T_x$, the energy dispersive spectra (EDS) images of $Ti_3C_2T_x$-CTAB showed the presence of N and Br elements of CTAB (Fig. 1e and Fig. S6 and S7, ESI†). Also, an additional C–N peak appeared in the high-resolution C 1s X-ray photoelectron spectroscopy (XPS) spectrum of $Ti_3C_2T_x$-CTAB (Fig. 1f).[24,25] In the Ti 2p XPS spectra, the decreased proportion of the Ti–C bond and the increased proportion of $Ti^{2+}/Ti^{3+}$ and Ti–O bonds in $Ti_3C_2T_x$-CTAB also confirmed the intercalation of CTAB (Fig. S8 and Table S2, ESI†).[24] All these results confirmed the successful intercalation of CTAB into $Ti_3C_2T_x$ MXene.

### Solid complexation effect between CTAB and bromine

The solid complexation effect between CTAB (namely $CTA^+$-$Br^-$) and bromine was investigated *via* Raman spectroscopy and XPS test. After the interaction of CTAB with bromine (denoted as $CTA^+$–$Br_n^-$, $n$ = 3 or 5), two novel peaks of $Br_3^-$ (159 $cm^{-1}$) and $Br_5^-$ (211 $cm^{-1}$) appeared in the Raman spectra of $CTA^+$–$Br_n^-$, indicating the successful bromine complexation (Fig. 2a and Fig. S9, ESI†).[26–28] In the C 1s XPS spectra of CTAB, the peak of C–$N^+$ was found at 285.89 eV, which shifted to a higher energy (286.05 eV) than that of $CTA^+$–$Br_n^-$ (Fig. 2b). The C–$N^+$ peak in the N 1s XPS spectra also exhibited a positive shift of 0.07 eV (Fig. S10, ESI†).[29,30] These positive shifts were because that the electron cloud density of the C–N bond decreased when $CTA^+$ was combined with $Br_n^-$ (Fig. S9, ESI†). Moreover, in the high-resolution Br 3d XPS spectra of $CTA^+$–$Br_n^-$, the emerging peaks at 68.95 and 70.30 eV were assigned to $Br_3^-$ and $Br_5^-$, respectively, further verifying the bromine complexation effect of CTAB (Fig. 2c).[21,31] The bromine content in EDS energy spectra obviously increased from 3.52% in CTAB to 7.35% in $CTA^+$–$Br_n^-$, confirming Raman and XPS results (Fig. S11 and Table S3, ESI†). As a result, CTAB can play the same role as that of BCAs in inhibiting bromine diffusion/crossover.

To study the complexing power of CTAB, we used MEPBr for comparison, which is nowadays the most commonly used BCA. When adding MEPBr to a bromine solution, an oily $MEP^+$–$Br_n^-$ phase was formed and the aqueous solution (labelled as solution A) color turned clear but still yellow after 12 h (Fig. S12, ESI†). However, in the same solution containing CTAB, the yellow solid bromine complexes were formed, while the aqueous solution (labelled as solution B) was almost colorless, indicating the dramatically decreased bromine concentration in the aqueous phase (Fig. S12, ESI†). Then, the UV-vis spectra were utilized to quantitatively analyse the bromine species in solutions A and B, respectively (Fig. 2d and Fig. S12b, ESI†). The intensities of bromine species in solution B were so low as to be almost undetectable, which were much lower than that of solution A even after 10 times dilution (Fig. 2d). Furthermore, CTAB could capture bromine species from the oily $MEP^+$–$Br_n^-$ phase and then almost completely transferred to the solid $CTA^+$–$Br_n^-$ phase, however which was an irreversible process (Fig. 2e). All these comparisons indicated that CTAB had a stronger complexing effect on bromine species than that of MEPBr.[32,33]

To further confirm this, density functional theory (DFT) calculations were carried out to calculate the Gibbs free-energy changes ($\Delta G$s) between MEPBr/CTAB and $Br_2$ (Fig. 2f–g and

 

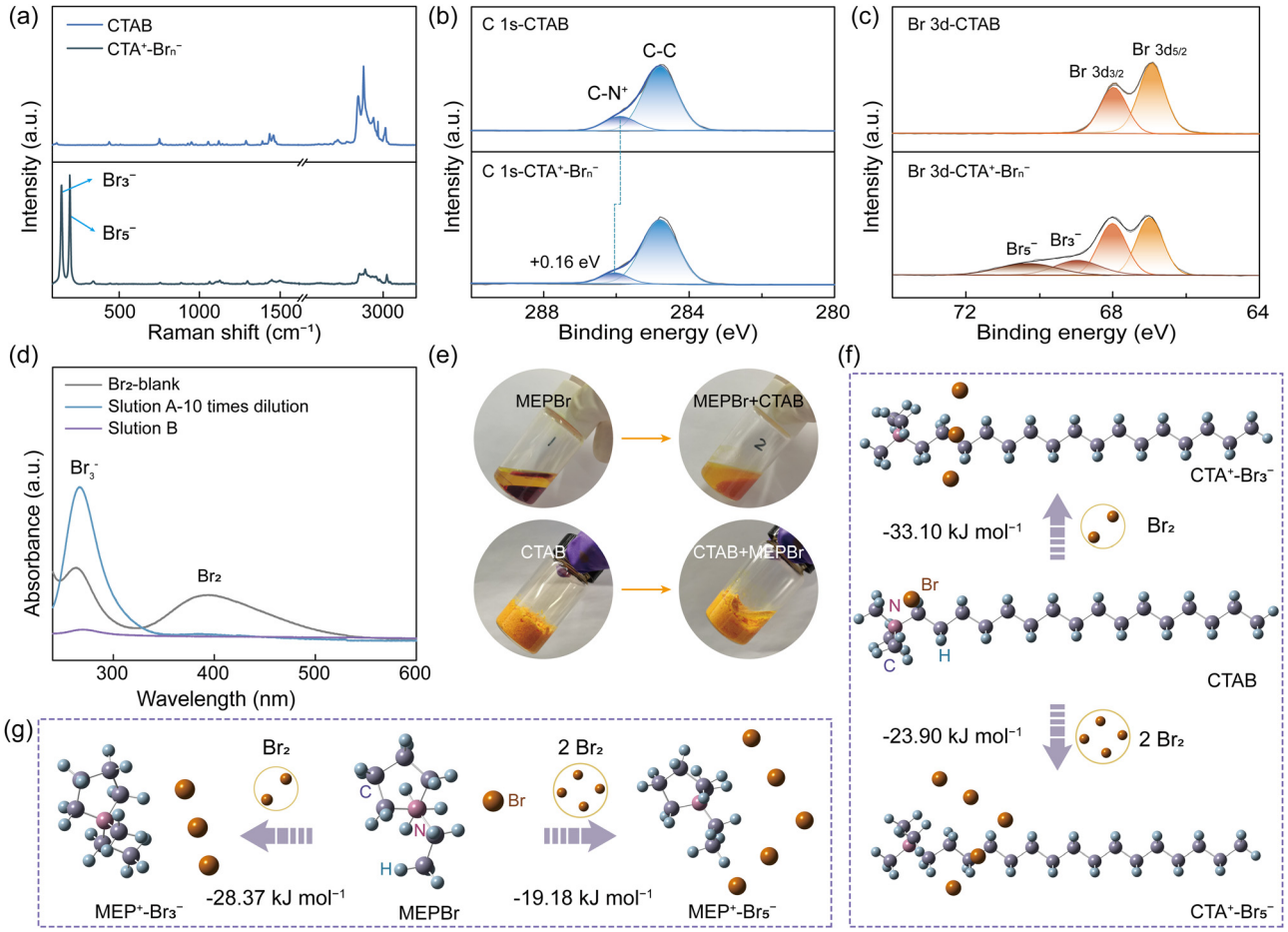


Fig. 2 Verification of the solid bromine complexation effect of CTAB. (a) Raman spectra of CTAB and $CTA^+$–$Br_n^-$. High-resolution (b) C 1s and (c) Br 3d XPS spectra of CTAB and $CTA^+$–$Br_n^-$. (d) UV-vis spectra of different aqueous bromine solutions. (e) Photographs of the bromine complexes before and after adding the aqueous CTAB solution to $MEP^+$–$Br_n^-$ (up) and the aqueous MEPBr solution to $CTA^+$–$Br_n^-$ (down). The formation processes of (f) $CTA^+$–$Br_n^-$ and (g) $MEP^+$–$Br_n^-$ and the corresponding $\Delta G$s of reactions.

Table S4, ESI†). The $\Delta G$ of MEPBr with $Br_2$ was −28.37 kJ $mol^{-1}$, higher than that of CTAB (−33.10 kJ $mol^{-1}$), indicating the stronger bromine complexing capacity of CTAB. Also, the $\Delta G$ values of forming $MEP^+$-$Br_5^-$ and $CTA^+$-$Br_5^-$ complexes were −19.18 kJ $mol^{-1}$ and −23.90 kJ $mol^{-1}$, respectively, further implying the superiority of CTAB (Fig. 2f–g and Table S4, ESI†). Furthermore, at higher temperatures of 50 °C and 70 °C, bromine clearly volatilized from the oily $MEP^+$–$Br_n^-$ phase (Fig. S13, ESI†). In contrast, very rare bromine vapor could be observed from the solid $CTA^+$–$Br_n^-$ complexes, proving that this solid complexation effect of CTAB was more robust even at high temperatures.

### Effects of the solid complexation on the electrochemical performance

An adverse effect of the solid complexation is the probably decreased reaction kinetics of the $Br_2/Br^-$ redox couple (Fig. S14, ESI†).[13,20] Thus, we used $Ti_3C_2T_x$ MXene with excellent electronic conductivity, high hydrophilicity and plentiful active sites as a carrier to combine CTAB and a PCF substrate.[34–36] Especially, $Ti_3C_2T_x$ MXene also exhibited very low adsorption energies ($\Delta E$s) to bromine, indicating great bromine adsorption capacity (Fig. 3a and Fig. S15, ESI†). Considering that the rate-determining step of $Br_2/Br^-$ reactions is to form $Br_{ads}$ at the adsorbed state, $Ti_3C_2T_x$ MXene can thus expedite $Br_2/Br^-$ reactions, which is a prerequisite for being a carrier of CTAB. Moreover, the expanded interlayer spacing dramatically increased the specific surface area of $Ti_3C_2T_x$-CTAB (Fig. S16, ESI†). More active sites were exposed and the mass transfer was accelerated, further enhancing its electrochemical performance (Fig. S17, ESI†).

The electrocatalytic properties of $Ti_3C_2T_x$ and $Ti_3C_2T_x$-CTAB were then evaluated *via* cyclic voltammetry (CV), linear sweep voltammetry (LSV) and electrochemical impedance spectroscopy (EIS), which were loaded on pristine glassy carbon (PGC) substrates (denoted as TiGC and TiCGC, respectively). As shown in Fig. 3b, the higher cathodic peak current ($I_c$) of TiGC than that of PGC suggested the high catalytic activity of $Ti_3C_2T_x$ MXene carriers in $Br_2/Br^-$ reactions. However, even though the solid $CTA^+$–$Br_n^-$ complexes were formed, TiCGC still exhibited the highest $I_c$, namely the best electrochemical activity. Moreover, the slopes of the LSV curves followed the

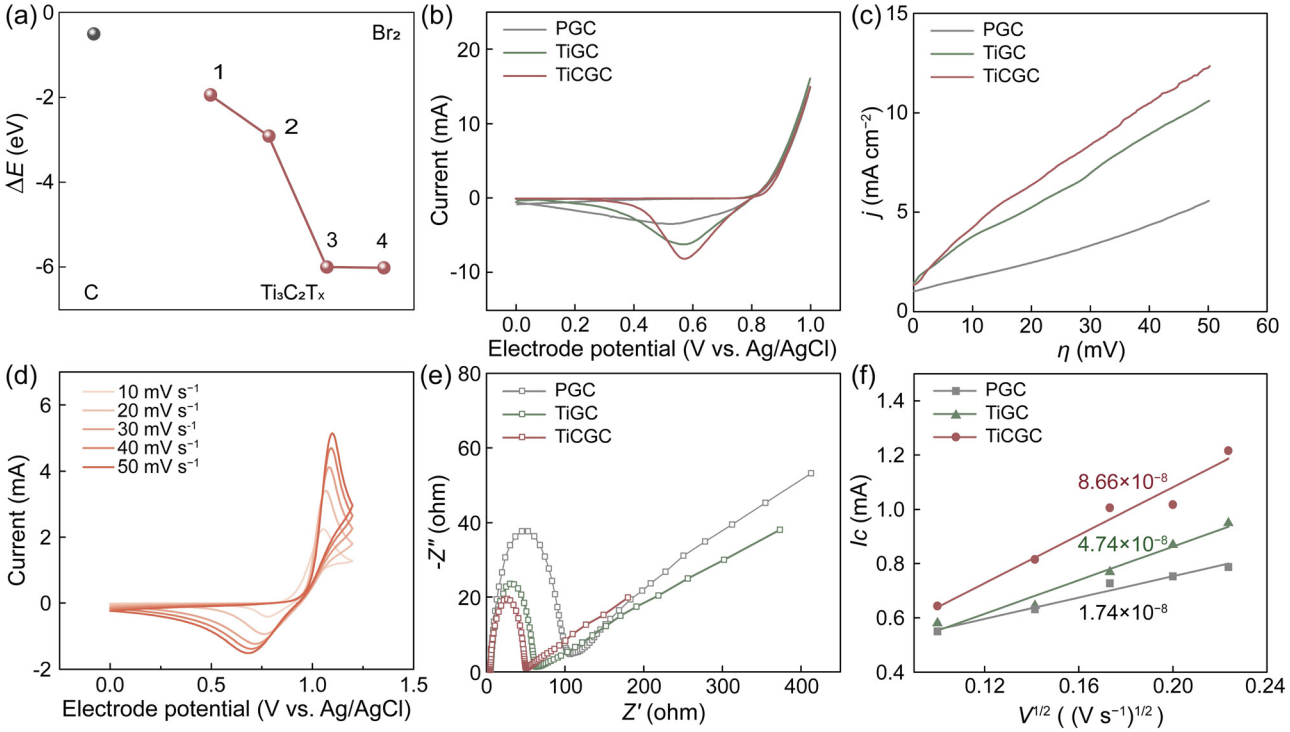


Fig. 3 Electrochemical performance and the bromine affinity of $Ti_3C_2T_x$-CTAB. (a) The $\Delta E$s of bromine molecules adsorbed on different Ti sites of $Ti_3C_2T_x$ MXene. (b) CV curves at a scan rate of 10 mV $s^{-1}$. (c) LSV curves at a scan rate of 1 mV $s^{-1}$. (d) CV curves of TiCGC at different scan rates. (e) Nyquist plots. (f) Relationships between the $I_c$ and the square root of the scan rate ($v^{1/2}$).

order of TiCGC > TiGC > PGC, also indicating the fastest reaction kinetics of the $Br_2/Br^-$ redox couple on $Ti_3C_2T_x$-CTAB (Fig. 3c). The resultant kinetic parameters, including the exchange current density ($i_0$) and rate constant for the reaction ($k_0$) of TiCGC, were also the highest, quantifying the significant improvement in reaction kinetics (Table S5, ESI†). As a result, in Br-FBs, the reaction kinetics of the $Br_2/Br^-$ redox couple would not be affected by the solid complexation of CTAB but enhanced based on the high electrochemical activity of $Ti_3C_2T_x$ MXene carriers. Most importantly, as the scan rate increased, the anodic peak potential shifted positively and the cathodic peak potential shifted negatively, indicating the reversible solid complexation of CTAB with bromine (Fig. 3d). Namely, the solid $CTA^+$–$Br_n^-$ complexes could release the soluble bromine species during the discharge process (Scheme 1). Moreover, the steady activity for 500 cycles further indicated that $Ti_3C_2T_x$-CTAB was electrochemically stable (Fig. S18, ESI†). Meanwhile, the interlayer spacing, structure and electrochemical activity of $Ti_3C_2T_x$-CTAB almost did not change before and after reacting with bromine, showing its high oxidization stability and anti-stack ability (Fig. S19 and S20, ESI†).

The Nyquist plots in Fig. 3e all included semicircles and liner parts, attributing to the electron transfer process at high frequencies and the diffusion process at low frequencies, respectively.[8] The smallest semicircle radius of TiCGC indicated its lowest charge transfer resistance, supporting the CV and LSV results. Furthermore, the calculated diffusion coefficient of $Br_2$ on TiCGC ($8.66 \times 10^{-8}$ cm $s^{-1}$) was higher than that of TiGC ($4.74 \times 10^{-8}$ cm $s^{-1}$), indicating the better mass transfer capacity of $Ti_3C_2T_x$-CTAB due to the intercalation (Fig. 3f and Table S6, ESI†). This was another reason why $Ti_3C_2T_x$-CTAB displayed better electrochemical performance than $Ti_3C_2T_x$.

### Bromine capture capacity of $Ti_3C_2T_x$-CTAB

Notably, the bromine complexation effect of CTAB and the bromine adsorption effect of $Ti_3C_2T_x$ MXene carriers could jointly contribute to the excellent bromine entraping/retention capacity of $Ti_3C_2T_x$-CTAB, then inhibiting bromine diffusion/crossover. We first applied a stationary visualization experiment to support this. From Fig. 4a, after adding $Ti_3C_2T_x$ and $Ti_3C_2T_x$-CTAB to bromine solution, respectively, the solution color became clearer and clearer as prolonging the time. Nonetheless, the solution containing $Ti_3C_2T_x$-CTAB was always the clearest because of the stronger complexation effect of the intercalated CTAB. The higher stability of $Ti_3C_2T_x$-CTAB-$Br_2$ than that of $Ti_3C_2T_x$-$Br_2$ at a high temperature of 50 °C further proved the effectiveness and robustness of such a solid complexation effect (Fig. S21, ESI†). In another words, the strong and stable bromine complexation capacity of CTAB played the dominant role in entrapping bromine species. Then, the rotating ring-disk electrode technique was used to interpret their bromine entrapping capacities. In Fig. 4b, the $|I_{ring}|$ represented the bromine entrapping capability of different materials, which was determined by the bromine diffused to the ring electrode. Compared with the substrate, the $|I_{ring}|$ of $Ti_3C_2T_x$

 

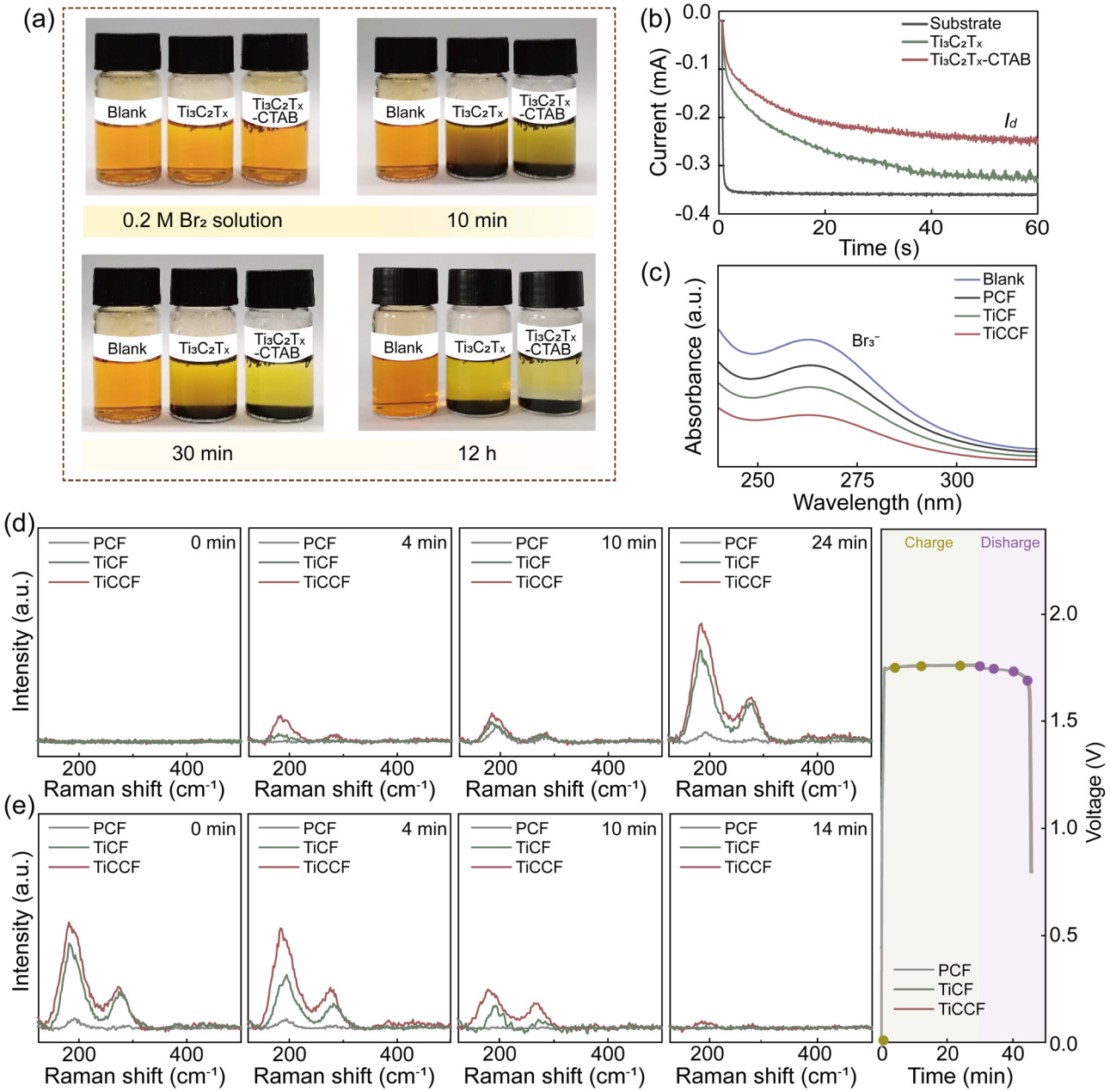


Fig. 4 Bromine capturing capacity tests and species changes on electrodes during electrochemical reactions. (a) Photographs of the color changes of bromine solutions over time after adding different materials. (b) $I_{ring}$–$t$ curves of different materials. (c) UV-vis spectra of bromine solution after immersing PCF, TiCF and TiCCF. *In situ* Raman spectra on different cathodes of ZBFBs during the (d) charge and (e) discharge processes at different time intervals.

was reduced by adsorbing bromine. The lowest $|I_{ring}|$ of $Ti_3C_2T_x$-CTAB validated its best capacity to entrap bromine, which was mainly due to the powerful complexation effect of CTAB.

We then loaded $Ti_3C_2T_x$-CTAB onto a PCF substrate to construct a composite electrode (denoted as TiCCF) and investigate its application in Br-FBs. The decreased absorbance intensity in UV-vis spectra represented that bromine in the solution was entrapped in different electrodes (Fig. 4c).[33] Unsurprisingly, compared with the $Ti_3C_2T_x$-modified electrode (denoted as TiCF), TiCCF captured the most bromine (Fig. 4c). Also, from the *in situ* visualization experiment, bromine diffused rapidly from the PCF cathode to the anode, while the least bromine diffused from the TiCCF cathode no matter with or without BCAs, confirming the outstanding capacity of TiCCF to inhibit bromine diffusion/crossover (Fig. S22–S24, ESI†).

To gain deeper insights into the electrocatalytic behavior and bromine immobilization capacity of TiCCF, *in situ* Raman spectra were collected during the charge and discharge processes. As shown in Fig. 4d and e, the peaks of symmetrical stretching modes υ1 of $Br_3^-$ (199 $cm^{-1}$) and $Br_5^-$ (291 $cm^{-1}$)

were detected mainly due to the combination of $Br_2$ and $Br^-$.[12,37] As charging continued, $Br_5^-$ appeared and the peak intensities of $Br_3^-$ and $Br_5^-$ gradually increased. Compared with PCF and TiCF, TiCCF always exhibited the highest peak intensities of $Br_n^-$, confirming its best electrochemical activity and bromine retention capacity (Fig. 4d). Meanwhile, the intensity of $Br_3^-$ on TiCCF was always much higher than that of $Br_5^-$, which was mainly because that more $Br_2$ complexed with CTAB instead of combining with $Br_3^-$. Namely, more $Br_2$ could be encapsulated and retained in the TiCCF electrode, effectively preventing the bromine crossover. During the discharge process, the intensities of $Br_3^-$ and $Br_5^-$ peaks gradually declined and nearly vanished with the reduction of $Br_2$. Similarly, TiCCF still always displayed the highest peak intensities of $Br_n^-$ due to the fact that bromine species were entrapped and hardly diffused to the negative side. The nearly disappeared $Br_n^-$ peaks on TiCCF also indicated that the solid bromine complexation of CTAB was indeed reversible (Fig. 4d and e).

### Practical applications of TiCCF in Br-FBs

In general, solid bromine complexes in electrolytes will block the pipeline, which are consequently applied to single-flow or static bromine-based batteries generally (Fig. S14, ESI†).[13,20] However, solid $CTA^+$–$Br_n^-$ complexes in the electrode did not affect the flow of the electrolyte. As a result, TiCCF was used in ZBFBs (double-flow) to study its availability in Br-FBs at 40 mA h $cm^{-2}$ (Scheme 1). We first constructed a ZBFB using a TiCCF cathode, a PCF anode and electrolytes without BCAs (denoted as BCA-free

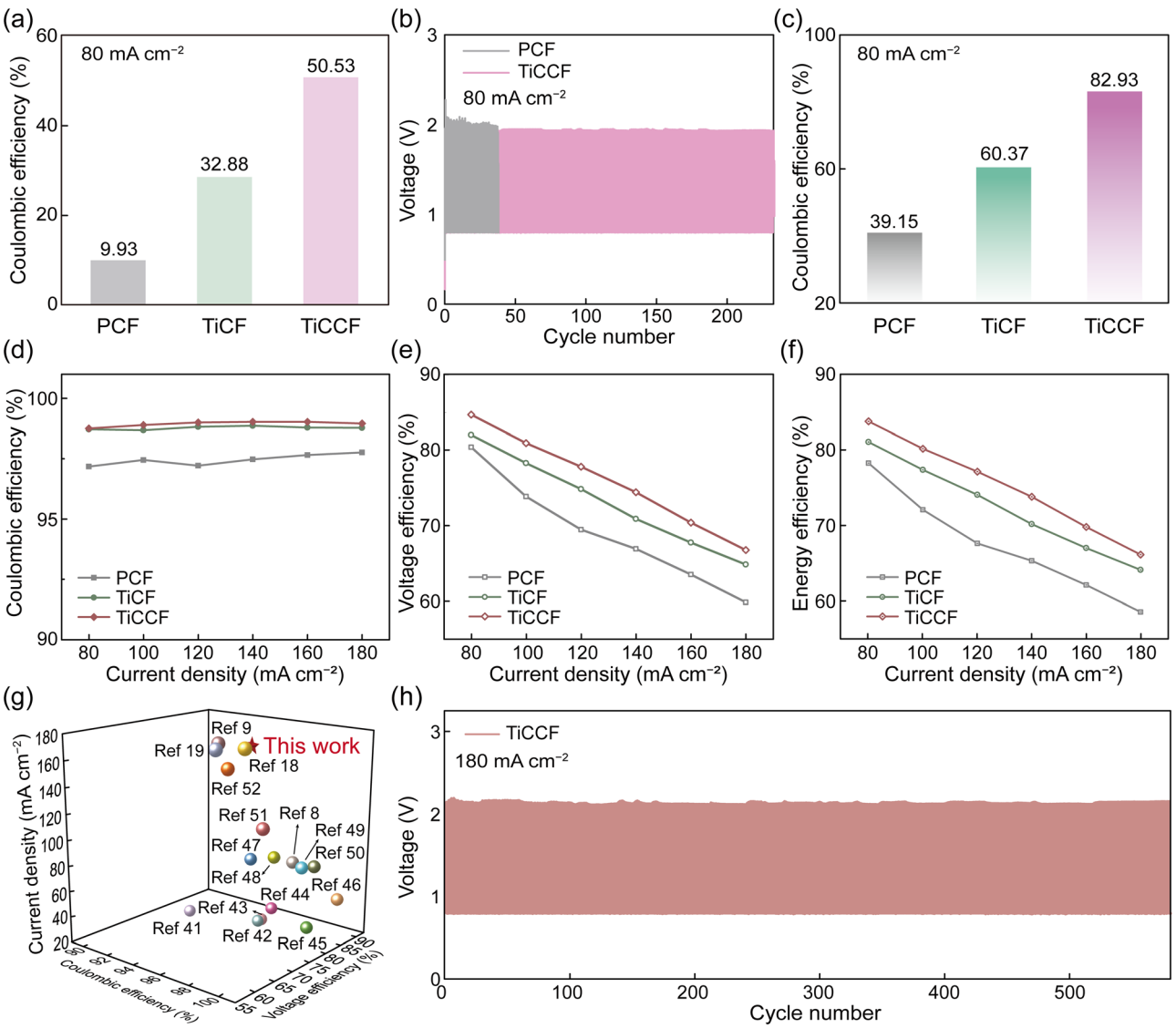


Fig. 5 Performance of ZBFBs with different electrodes. (a) The self-discharge performance of BCA-free ZBFBs with different cathodes at 80 mA $cm^{-2}$. (b) Cycling performance of BCA-free ZBFBs using different cathodes at 80 mA $cm^{-2}$. (c) The self-discharge performance of ZBFBs assembled with different cathodes at 80 mA $cm^{-2}$. The performance of ZBFBs assembled with different cathodes at different current densities: (d) CE, (e) VE, and (f) EE. (g) Comparisons of reported current densities and efficiencies of ZBFBs (all values derived from ref. 8, 9, 18, 19 and 41–52). (h) Charge–discharge curves of the ZBFB using the TiCCF cathode at 180 mA $cm^{-2}$.

 

ZBFB), which showed a high capacity retention rate of 50.53% after a standing test for 24 h at 80 mA $cm^{-2}$ (Fig. 5a). This much higher capacity retention rate than that of the current BCA-free ZBFB using the PCF cathode (only 9.93%) certified the potential of using the TiCCF cathode to suppress self-discharge. Additionally, in Fig. 5b and Fig. S25 (ESI†), TiCCF enabled the BCA-free ZBFB to maintain higher and more stable efficiencies for 233 cycles (232 h) at 80 mA $cm^{-2}$, showing its excellent stability. Of note, there was no electrolyte diffusion from the positive side to the negative side or corrosion of the graphite plate at the positive side in this BCA-free ZBFB after long cycling, benefiting from the excellent bromine entrapping capacity of $Ti_3C_2T_x$-CTAB on TiCCF (Fig. S26–S27, ESI†). Most importantly, the reversible solid bromine complexation of highly electrochemically active $Ti_3C_2T_x$-CTAB would not harm the reaction kinetics of the $Br_2/Br^-$ couple (Fig. S28 and Table S7, ESI†).[38,39] The BCA-free ZBFB based on the TiCCF cathode delivered a CE of 97.38% and a VE of 62.37% at a high current density of 200 mA $cm^{-2}$. This battery retained stable performance for 400 cycles, in favor of improved power density and capacity maintenance (Fig. S29, ESI†). Most importantly, as shown in Fig. 5c, even though adding MEPBr into electrolytes, the capacity retention rate (39.15%) of the ZBFB based on the PCF cathode was still much lower than that of the BCA-free ZBFB using the TiCCF cathode. These results verified the much stronger bromine complexation capacity of CTAB than that of MEPBr, indicating the potential for CTAB into electrodes to replace MEPBr into electrolytes. Additionally, the electrochemical stability of the TiCCF electrode in the highly corrosive bromine solution without BCAs also confirmed its superiority in practical applications (Fig. S30a, ESI†).

It was worth noting that the current ZBFB systems in the demonstration stage utilized MEPBr as the BCA in electrolytes, and the self-discharge of the aforementioned BCA-free ZBFB was still relatively high. Consequently, to improve the feasibility of TiCCF cathodes in practical applications, TiCCF cathodes were utilized in ZBFBs using electrolytes with MEPBr. Notably, the TiCCF electrode also exhibited the stable electrochemical performance in the electrolyte with MEPBr, ensuring its availability (Fig. S30b, ESI†). The assembled ZBFB demonstrated an ultrahigh capacity retention rate of 82.93% at 80 mA $cm^{-2}$, indicating the ultralow self-discharge of this battery (Fig. 5c). This capacity retention rate was more than twice higher than the current ZBFB system using the PCF cathode and MEPBr in electrolytes (39.15%), further confirming the outstanding bromine complexation capacity of CTAB. For the TiCF cathode, the capacity retention rate of the assembled ZBFB was 60.37%, due to the lack of such a strong CTAB complexation effect. Moreover, over the testing current density range from 80 to 180 mA $cm^{-2}$, the ZBFB assembled with the TiCCF cathode always delivered the highest efficiencies (Fig. 5d–f). The higher CE was mainly due to the high capacity retention rate and the excellent electrochemical reversibility, which was caused by the superior properties of $Ti_3C_2T_x$-CTAB. The higher VE was because of the significantly decreased polarization resulting from the best electrochemical performance of TiCCF (Fig. S31 and S32 and Table S7 and S8, ESI†).[40] Especially, its CE, VE and EE reached 98.95%, 66.76% and 66.06% at 180 mA $cm^{-2}$, respectively. The VE and EE were the highest values for ZBFBs ever reported at such a high current density, contributing to higher power density (Fig. 5g and Table S1, ESI†). Additionally, the remarkable cycling stability for 580 cycles (262 h) with stable efficiencies at 180 mA $cm^{-2}$ suggested that this ZBFB manifested efficient utilization of bromine species during the reversible electrochemical processes (Fig. 5h and Fig. S33, ESI†). The above results validated the superiority and practicability of TiCCF electrodes with considerable catalytic activity and bromine entrapping capacity in Br-FBs. Notably, compared with BCA-free ZBFBs, the VE and EE decreased at 180 mA $cm^{-2}$ (Fig. S34, ESI†). These were because of the increased battery polarization caused by introducing MEPBr (Fig. S28, S30, and S31, ESI†). Consequently, more efforts still need to be made on more effective and simple electrode strategies in order to construct BCA-free Br-FBs with lower self-discharge and higher power density.

## Conclusions

In summary, we proposed to introduce CTAB as the BCA onto $Ti_3C_2T_x$ MXene carriers to be electrodes for Br-FBs in order to reduce the self-discharge. The robust and reversible solid complexation effect of CTAB effectively entrapped bromine species into electrodes, inhibiting bromine diffusion/crossover more effectively. Meanwhile, the good bromine adsorption capacity of $Ti_3C_2T_x$ MXene carriers accelerated the reaction kinetics of the $Br_2/Br^-$ redox couple. Thus, the assembled ZBFB based on the $Ti_3C_2T_x$-CTAB modified cathode achieved an ultrahigh capacity retention rate of 82.93%, much higher than that of the current ZBFB system (39.15%). This battery also exhibited a high VE of 66.76% and a high EE of 66.06% at 180 mA $cm^{-2}$, in favor of higher power density. Furthermore, this ZBFB exhibited excellent cycling stability for 580 cycles with no obvious efficiency fading at 180 mA $cm^{-2}$. This work provides a valid access to construct Br-FBs with ultralow self-discharge, high power density and long lifespan based on electrode design, accelerating their further demonstration applications.

## Author contributions

Luyin Tang performed the experiments, analyzed the data and wrote the initial manuscript draft. Dr Tianyu Li conducted the DFT simulations. Dr Wenjing Lu and Prof. Xianfeng Li designed the experiments, participated in project planning and discussions of the results, and revised and finalized the manuscript for submission.

## Conflicts of interest

There are no conflicts to declare.

## Acknowledgements

This work was financially supported by the National Key R&D Program of China (2022YFB3805300), the National Natural Science Foundation of China (Grant No. 22379141 and 21935003), the International Partnership Program of Chinese Academy of Sciences (121421KYSB20210028), the Dalian Science and Technology Innovation Fund (2022JJ12GX024), and the Youth Innovation Promotion Association CAS (2022184). The authors would like to thank Congzhi Deng at DICP for the morphology test. Prof. Xianfeng Li acknowledged the financial support from XPLORER PRIZE.

## References

1 M. Armand and J.-M. Tarascon, *Nature*, 2008, **451**, 652–657.
2 Z. Zhao, X. Liu, M. Zhang, L. Zhang, C. Zhang, X. Li and G. Yu, *Chem. Soc. Rev.*, 2023, **52**, 6031–6074.
3 S. Chu, Y. Cui and N. Liu, *Nat. Mater.*, 2017, **16**, 16–22.
4 S. Chu and A. Majumdar, *Nature*, 2012, **488**, 294–303.
5 J. Noack, N. Roznyatovskaya, T. Herr and P. Fischer, *Angew. Chem., Int. Ed.*, 2015, **54**, 9776–9809.
6 L. Zhang, R. Feng, W. Wang and G. Yu, *Nat. Rev. Chem.*, 2022, **6**, 524–543.
7 Y. Zhang, F. Li, T. Li, M. Zhang, Z. Yuan, G. Hou, J. Fu, C. Zhang and X. Li, *Energy Environ. Sci.*, 2023, **16**, 231–240.
8 C. Wang, Q. Lai, P. Xu, D. Zheng, X. Li and H. Zhang, *Adv. Mater.*, 2017, **29**, 1605815.
9 W. Lu, P. Xu, S. Shao, T. Li, H. Zhang and X. Li, *Adv. Funct. Mater.*, 2021, **31**, 2102913.
10 K. Oh, A. Z. Weber and H. Ju, *Int. J. Hydrogen Energy*, 2017, **42**, 3753–3766.
11 X. Li, C. Xie, T. Li, Y. Zhang and X. Li, *Adv. Mater.*, 2020, **32**, 2005036.
12 X. Li, T. Li, P. Xu, C. Xie, Y. Zhang and X. Li, *Adv. Funct. Mater.*, 2021, **31**, 2100133.
13 L. Gao, Z. Li, Y. Zou, S. Yin, P. Peng, Y. Shao and X. Liang, *iScience*, 2020, **23**, 101348.
14 W. Lu, T. Li, C. Yuan, H. Zhang and X. Li, *Energy Storage Mater.*, 2022, **47**, 415–423.
15 L. Hua, W. Lu, T. Li, P. Xu, H. Zhang and X. Li, *Mater. Today Energy*, 2021, **21**, 100763.
16 M. Küttinger, P. A. Loichet Torres, E. Meyer, P. Fischer and J. Tübke, *Molecules*, 2021, **26**, 2721.
17 K. Saadi, M. Kuettinger, P. Fischer and D. Zitoun, *Energy Technol.*, 2021, **9**, 2000978.
18 L. Tang, T. Li, W. Lu and X. Li, *Sci. Bull.*, 2022, **67**, 1362–1371.
19 L. Tang, C. Liao, T. Li, C. Yuan, G. Li, W. Lu and X. Li, *Adv. Energy Mater.*, 2024, **14**, 2303282.
20 P. Xu, T. Li, Q. Zheng, H. Zhang, Y. Yin and X. Li, *J. Energy Chem.*, 2022, **65**, 89–93.
21 X. Li, N. Li, Z. Huang, Z. Chen, Y. Zhao, G. Liang, Q. Yang, M. Li, Q. Huang, B. Dong, J. Fan and C. Zhi, *ACS Nano*, 2021, **15**, 1718–1726.
22 J. Luo, C. Wang, H. Wang, X. Hu, E. Matios, X. Lu, W. Zhang, X. Tao and W. Li, *Adv. Funct. Mater.*, 2019, **29**, 1805946.
23 J. Luo, J. Zheng, J. Nai, C. Jin, H. Yuan, O. Sheng, Y. Liu, R. Fang, W. Zhang, H. Huang, Y. Gan, Y. Xia, C. Liang, J. Zhang, W. Li and X. Tao, *Adv. Funct. Mater.*, 2019, **29**, 1808107.
24 Z. Li, X. Wang, W. Zhang and S. Yang, *Chem. Eng. J.*, 2020, **398**, 125679.
25 K. Li, J. Zhao, A. Zhussupbekova, C. E. Shuck, L. Hughes, Y. Dong, S. Barwich, S. Vaesen, I. V. Shvets, M. Möbius, W. Schmitt, Y. Gogotsi and V. Nicolosi, *Nat. Commun.*, 2022, **13**, 6884.
26 G. Bauer, J. Drobits, C. Fabjan, H. Mikosch and P. Schuster, *J. Electroanal. Chem.*, 1997, **427**, 123–128.
27 M. E. Easton, A. J. Ward, B. Chan, L. Radom, A. F. Masters and T. Maschmeyer, *Phys. Chem. Chem. Phys.*, 2016, **18**, 7251–7260.
28 Y. Xu, C. Xie, T. Li and X. Li, *ACS Energy Lett.*, 2022, **7**, 1034–1039.
29 M. Foss, S. Diplas and E. Gulbrandsen, *Electrochim. Acta*, 2010, **55**, 4851–4857.
30 C. Wang, G. Ma, J. Zhou, M. Zhang, X. Ma, F. Duo, L. Chu, J. Huang and X. Su, *Appl. Organomet. Chem.*, 2019, **33**, e5077.
31 W. Cai, J. Wang, X. Quan and Z. Wang, *J. Appl. Polym. Sci.*, 2018, **135**, 45657.
32 Q. Liu and D. W. Margerum, *Environ. Sci. Technol.*, 2001, **35**, 1127–1133.
33 B. N. Grgur, *J. Electrochem. Soc.*, 2019, **166**, E50–E61.
34 Y. An, Y. Tian, H. Shen, Q. Man, S. Xiong and J. Feng, *Energy Environ. Sci.*, 2023, **16**, 4191–4250.
35 Y. Zhao, J. Zhang, X. Guo, X. Cao, S. Wang, H. Liu and G. Wang, *Chem. Soc. Rev.*, 2023, **52**, 3215–3264.
36 H. Wang, Z. Du, Z. Cheng, Z. Cao, Y. Ye, Z. Wang, J. Wei, S. Wei, X. Meng, L. Song, Y. Gong, S. Yang and L. Guo, *Adv. Mater.*, 2023, **35**, 2301399.
37 J.-H. Lee, Y. Byun, G. H. Jeong, C. Choi, J. Kwen, R. Kim, I. H. Kim, S. O. Kim and H.-T. Kim, *Adv. Mater.*, 2019, **31**, 1904524.
38 M. Schneider, G. P. Rajarathnam, M. E. Easton, A. F. Masters, T. Maschmeyer and A. M. Vassallo, *RSC Adv.*, 2016, **6**, 110548–110556.
39 S. S. Li, J. R. Sun and J. Q. Guan, *Chin. J. Catal.*, 2021, **42**, 511–556.
40 Y.-Q. Zhang, G.-X. Wang, R.-Y. Liu and T.-H. Wang, *Energies*, 2023, **16**, 3043.
41 W. I. Jang, J. W. Lee, Y. M. Baek and O. O. Park, *Macromol. Res.*, 2016, **24**, 276–281.
42 S. Suresh, M. Ulaganathan and R. Pitchai, *J. Power Sources*, 2019, **438**, 226998.
43 S. Suresh, M. Ulaganathan, R. Aswathy and P. Ragupathy, *ChemElectroChem*, 2018, **5**, 3411–3418.
44 K. Mariyappan, P. Ragupathy and M. Ulaganathan, *J. Electrochem. Soc.*, 2021, **168**, 090566.
45 R. P. Naresh, K. Mariyappan, K. S. Archana, S. Suresh, D. Ditty, M. Ulaganathan and P. Ragupathy, *ChemElectroChem*, 2019, **6**, 5688–5697.

 

46 K. Mariyappan, R. Velmurugan, B. Subramanian, P. Ragupathy and M. Ulaganathan, *J. Power Sources*, 2021, **482**, 228912.
47 K. Mariyappan, T. Mahalakshmi, T. S. Roshni, P. Ragupathy and M. Ulaganathan, *Adv. Mater. Interfaces*, 2023, **10**, 2202007.
48 C. Wang, X. Li, X. Xi, W. Zhou, Q. Lai and H. Zhang, *Nano Energy*, 2016, **21**, 217–227.
49 H. Jung, J. Lee, J. Park, K. Shin, H. T. Kim and E. Cho, *Small*, 2023, **19**, 2208280.
50 H. X. Xiang, A. D. Tan, J. H. Piao, Z. Y. Fu and Z. X. Liang, *Small*, 2019, **15**, 1901848.
51 R. Wang, *J. Energy Storage*, 2023, **74**, 109487.
52 C. Wang, W. Lu, Q. Lai, P. Xu, H. Zhang and X. Li, *Adv. Mater.*, 2019, **31**, 1904690.